PHYSICAL REVIEW D **92,** 114028 (2015)

Effect of $c\bar{c}$ resonances in the branching ratio and forward-backward asymmetry of the decay $B \to K^* \mu^+ \mu^-$

Mohammad Ahmady[*] and Dan Hatfield[†]
Department of Physics, Mount Allison University, Sackville, New Brunswick, Canada, E4L 1E6

Sébastien Lord[‡]
Département de Mathématiques et Statistique, Université de Moncton, Moncton, New Brunswick, Canada, E1A 3E9

Ruben Sandapen[§]
Department of Physics, Acadia University, Wolfville, Nova-Scotia, Canada, B4P 2R6 and Department of Physics, Mount Allison University, Sackville, New Brunswick, Canada, E4L 1E6

(Received 12 August 2015; published 23 December 2015)

We compute the branching ratio and forward-backward asymmetry ($A_{\rm FB}$) distribution for the rare dileptonic decay $B \to K^* \mu^+ \mu^-$ for the full range of q^2, the dimuon mass squared, region. For the required form factors, we use nonperturbative inputs as predicted by the anti-de Sitter (AdS)/QCD correspondence. When using the Breit-Wigner model with momentum-dependent decay constants to account for the ψ and ψ' resonance effects in the nonresonance region of the spectrum, we find our predictions to be in better agreement with the experimental data for the branching ratio.

DOI: 10.1103/PhysRevD.92.114028 PACS numbers: 12.38.-t, 13.20.He

I. INTRODUCTION

The rare decay $B \to K^* \mu^+ \mu^-$ has recently been attracting much attention from both the experimental [1–9] and theoretical [10–21] sides due to the various observables associated with this decay that are susceptible to reveal new physics (NP). In particular, Ref. [11] has brought to light an overall tension between the Standard Model predictions and the experimental data and has suggested that a modification to the $C_{7,9}$ Wilson coefficients could resolve this tension.

To investigate signals of NP, one usually focuses on the region of the spectrum away from ψ and ψ' resonances where short-distance (SD) interactions, as represented by Figs. 1(a) and 1(b), are dominant. Experimentally, the q^2 region around the above two resonances are subtracted from the dileptonic spectrum. However, a careful analysis of $B \to K^* \mu^+ \mu^-$ observables should consider the long-distance effects of the resonances in the SD dominated region. In this paper, we take into account the narrow resonance effects in the nonresonance region when calculating the differential decay rate and the forward-backward asymmetry in this decay. In doing so, we use a Breit-Wigner model for the resonances with momentum-dependent decay constants [22]. We note that the latter model fits the data on photoproduction and the leptonic width of ψ and ψ' simultaneously [23] and is used for exclusive $B \to K^* \mu^+ \mu^-$ for the first time. The effects of broad resonances, using quark hadron duality, are considered in Ref. [18,24].

In a previous paper [25], we have computed the full set of seven independent $B \to K^*$ transition form factors. At low-to-intermediate q^2, we used light-cone sum rules with AdS/QCD distribution amplitudes (DAs) [26]. These DAs are derived from the holographic AdS/QCD light-front wave function for K^* [27,28]. We have fitted these with form factor predictions at high q^2 from lattice QCD. In this work, the same method for the derivation of the form factors with updated inputs (B meson decay constant f_B and b-quark mass m_b) is used to calculate the differential branching ratio and forward-backward asymmetry in the decay $B \to K^* \mu^+ \mu^-$.

We find that including the resonance effects improves the agreement of our predictions with the LHCb data [1] and the latest CMS data [9] on the differential branching ratio. As for $A_{\rm FB}$, it seems that the inclusion of the resonances hardly changes our prediction for the dimuon mass squared below the first resonance. Finally, we find that a negative shift in the Wilson coefficient C_9 enhances the agreement with the data for the differential branching ratio and the $A_{\rm FB}$ at q^2 below the first $c\bar{c}$ resonance.

II. DIFFERENTIAL BRANCHING RATIO WITH RESONANCES

In our previous paper [25], we calculated the differential branching ratio for $B \to K^* \mu^+ \mu^-$ without considering the effects of resonances. The inclusion of ψ and ψ' resonances, as illustrated in Fig. 1(c), is obtained by

[*]mahmady@mta.ca
[†]dhatfield@mta.ca
[‡]esl8420@umoncton.ca
[§]rsandapen@mta.ca

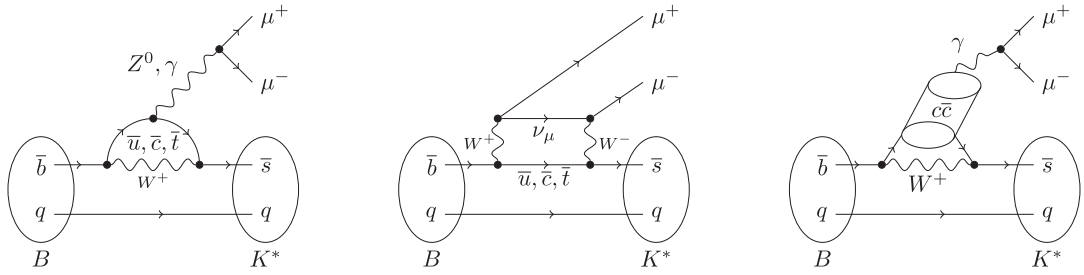

(a) SD penguin diagram (b) SD box diagram (c) LD resonance diagram

FIG. 1. Feynman diagrams of the principal contributions to the $B \to K^* \mu^+ \mu^-$ decay.

modifying C_9^{eff} with an additional term C_9^{res} which, using the Breit-Wigner model, can be written as [29,30]

$$C_9^{\text{res}} = (3C_1(\mu) + C_2(\mu)) \times \frac{16\pi^2}{9}\left(\frac{f_\psi^2/m_\psi^2}{m_\psi^2 - q^2 - i m_\psi \Gamma_\psi} + (\psi \to \psi')\right), \quad (1)$$

where C_1 and C_2 are the Wilson coefficients corresponding to the current-current operators O_1 and O_2 evaluated at scale $\mu \sim m_b$ and $f_{\psi^{(\prime)}}$ and $\Gamma_{\psi^{(\prime)}}$ are the decay constant and total width of the $c\bar{c}$ resonance $\psi^{(\prime)}$, respectively. We use the same convention for the effective operators as in Ref. [31] and the following definition for the vector meson decay constant:

$$\langle 0|\bar{c}\gamma_\mu c|V\rangle = f_V \epsilon_\mu. \quad (2)$$

Since ψ and ψ' resonances are off mass shell for q^2 different from $m^2_{\psi^{(\prime)}}$ in $B \to K^* \mu^+ \mu^-$, we need to consider the q^2-dependence of their decay constants [22]

$$f_V(q^2) = f_V(0)\left(1 + \frac{q^2}{c_V}[d_V - h(q^2)]\right) \quad (V = \psi, \psi') \quad (3)$$

with the h function being related to the imaginary part of the quark-loop diagram,

$$h(q^2) = \frac{1}{16\pi^2 r} \times \left(-4 - \frac{20r}{3} + 4(1+2r)\sqrt{1-\frac{1}{2}}\arctan\frac{1}{\sqrt{1-\frac{1}{r}}}\right), \quad (4)$$

where $r = q^2/4m_q^2$ for $0 < q^2 < 4m_q^2$. m_q is the effective quark mass, and assuming that the vector mesons are weakly bound systems of a quark and an antiquark, we take $m_q = m_V/2$. As a result, Eq. (4), defined for $0 < q^2 < 4m_q^2$, is an interpolation of f_V from the experimental data on $f_V(0)$ (from photoproduction) and $f_V(m_V^2)$ (from leptonic width) based on a quark-loop diagram. We assume $f_V(q^2) = f_V(m_V^2)$ for $q^2 > m_V^2$. The numerical values of the parameters c_V and d_V in Eq. (3) are given in Table I [22].

The resonance contributions C_9^{res} augments the short-distance contributions C_9^{eff} in the effective Hamiltonian:

$$C_9^{\text{tot}} = C_9^{\text{eff}} - C_9^{\text{res}}. \quad (5)$$

The minus sign in Eq. (5) is due to our choice of convention for the Wilson coefficients. The real and imaginary components of C_9^{tot} as a function of q^2 are shown in Fig. 2. To calculate the differential branching ratio including the resonance contributions, one should replace C_9^{eff} by C_9^{tot} in the differential branching ratio expression given in Ref. [25].

As for the seven form factors which parametrize the $B \to K^*$ transition, they are calculated using AdS/QCD DAs [25] in conjunction with light-cone sum rules at low to intermediate q^2. For high q^2 values, we use the latest lattice data for $B \to K^*$ transition form factors [32]. Note that we use the lattice results reported under ensemble f0062 as they correspond to finer lattice spacing. We use the following two-parameter form to fit the form factors obtained from AdS/QCD at low-to-intermediate q^2 and the lattice data at high q^2:

$$F(q^2) = \frac{F(0)}{1 - a\frac{q^2}{m_B^2} + b\frac{q^4}{m_B^4}}. \quad (6)$$

The updated values for $F(0)$, a and b are given in Table II. Our prediction for the differential branching ratio including the effects of the resonances ψ and ψ' as obtained by using the above form factors is shown in Fig. 3 where we compare with the latest data from LHCb [1] and CMS [9]. Our numerical results are calculated with the input parameters given in Table III and the Wilson coefficients tabulated in Table IV. Figure 3 clearly shows the effect of including resonances

TABLE I. Parameters (in GeV-based units) used in the q^2 evolution of f_V.

V	$f_V(0)$	$f_V(m_V^2)$	c_V	d_V
ψ	0.54	1.25	0.54	0.77
ψ'	0.043	1.04	0.043	0.043

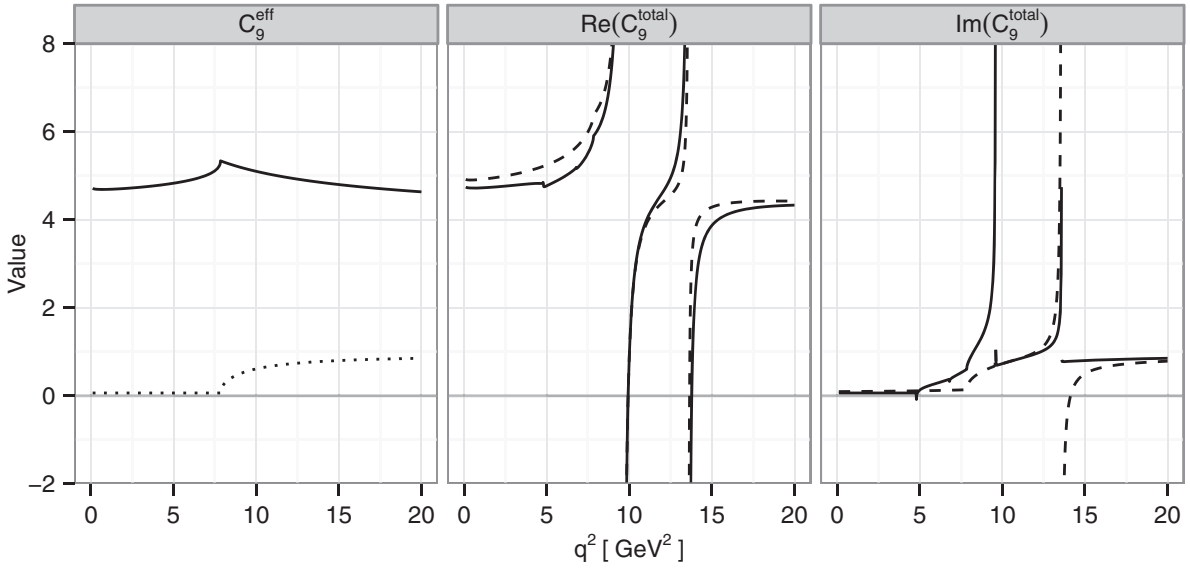

FIG. 2. Plots of $C_9^{\rm eff}$, $\Re(C_9^{\rm tot})$ and $\Im(C_9^{\rm tot})$ vs q^2. In the left plot, the solid curve is $\Re(C_9^{\rm eff})$ while the dotted curve is $\Im(C_9^{\rm eff})$. In the middle and right figures, the solid and dashed curves correspond to utilizing momentum-dependent and momentum-independent decay constants, respectively.

with the momentum-dependent decay constant on our prediction of the differential branching ratio.

III. FORWARD-BACKWARD ASYMMETRY

The forward-backward asymmetry distribution in dileptonic rare $B \to K^*\mu^+\mu^-$ decay is defined as

$$\frac{dA_{\rm FB}}{dq^2} \equiv \frac{1}{d\Gamma/dq^2} \times \left(\int_0^1 d(\cos\theta_\ell) \frac{d^2\Gamma}{dq^2 d\cos\theta_\ell} - \int_{-1}^0 d(\cos\theta_\ell) \frac{d^2\Gamma}{dq^2 d\cos\theta_\ell} \right), \tag{7}$$

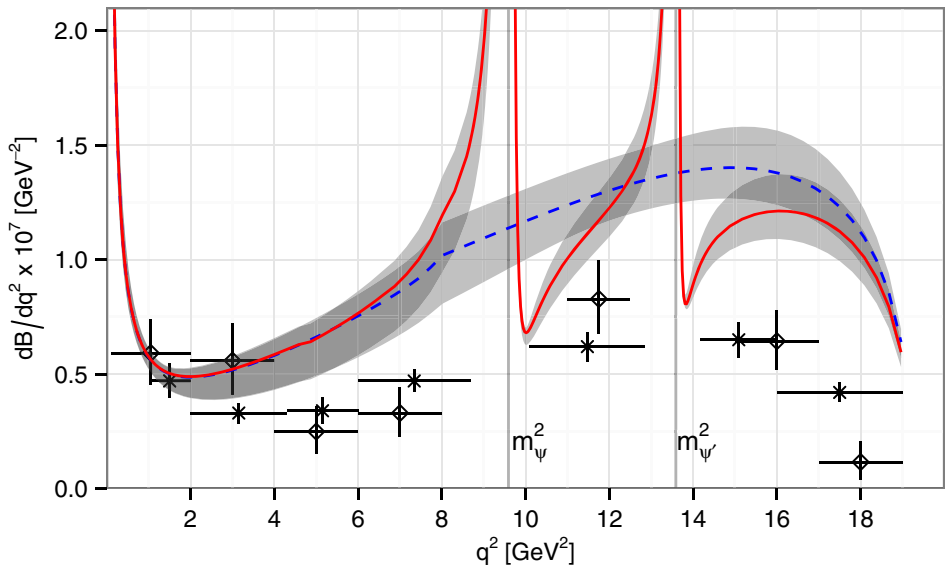

FIG. 3 (color online). The AdS/QCD prediction for the differential branching ratio of the $B \to K^*\mu^+\mu^-$ decay, with (solid red) and without (dashed blue) resonances, as compared with the latest LHCb [$B^+ \to K^{*+}\mu^+\mu^-$ (diamonds)] and CMS [$B^0 \to K^{*0}\mu^+\mu^-$ (crosses)] data. Note that this plot is qualitative, and our predictions for each experimental bin for this observable are shown in Table V in Appendix.

TABLE II. Updated fit parameters for the seven independent $B \to K^*$ form factors used in Eq. (6).

F	A_0	A_1	A_2	T_1	T_2	T_3	V
$F(0)$	0.243	0.244	0.244	0.258	0.239	0.157	0.297
a	1.618	0.586	1.910	1.910	0.525	1.147	1.934
b	0.561	−0.356	1.498	1.082	−0.459	−0.114	1.089

TABLE III. Numerical values of the input parameters used in our calculations.

$m_q = 0.35$ GeV	$m_B = 5.28$ GeV
$m_s = 0.48$ GeV	$m_{K^*} = 0.89$ GeV
$m_c = 1.4$ GeV	$m_\psi = 3.10$ GeV
$m_b = 4.6$ GeV	$m_{\psi'} = 3.69$ GeV
$m_t = 173.5$ GeV	
$\alpha_s(m_Z) = 0.1185$	$m_Z = 91.19$ GeV
$\alpha_{em} = 1/133$	
$f_{K^*}^\perp = 0.119$ GeV	$M_B(\text{Borel}) = 8$ GeV
$f_{K^*} = 0.225$ GeV	$s_0 = 36$ GeV
$f_B = 0.18$ GeV	

TABLE IV. Values of the Wilson coefficients at $\mu = m_b$.

C_1	C_2	C_3	C_4	C_5	C_6	C_7^{eff}	C_8^{eff}	C_9	C_{10}
−0.148	1.060	0.012	−0.035	0.010	−0.039	−0.307	−0.169	4.238	−4.641

where θ_ℓ is the angle between the positive muon and the line of flight of K^* in the $\mu^+\mu^-$ rest frame. This distribution to next-to-leading order (NLO) accuracy in α_s is given by [31]

$$\begin{aligned}\frac{dA_{FB}}{dq^2} = &-\frac{1}{d\Gamma/dq^2}\frac{G_F^2|V_{ts}^*V_{tb}|^2}{128\pi^3}m_B^3\lambda(q^2,m_{K^*}^2)^2\left(\frac{\alpha_{em}}{4\pi}\right)^2\\ &\times C_{10}A_1(q^2)V(q^2)\Re\left[\left(C_9^{\text{tot}}+\frac{\alpha_s C_F}{4\pi}C_\perp^{(\text{nf},9)}(q^2)\right)\right.\\ &+\frac{\hat{m}_b}{q^2}\left((m_B+m_{K^*})\frac{T_1(q_2)}{V(q^2)}+(m_B-m_{K^*})\frac{T_2(q^2)}{A_1(q^2)}\right)\\ &\times\left(C_7^{\text{eff}}+\frac{\alpha_s C_F}{4\pi}C_\perp^{(\text{nf},7)}(q^2)\right)+\frac{\hat{m}_b}{q^2}\left((m_B+m_{K^*})\frac{1}{V(q^2)}\right.\\ &\left.+(m_B-m_{K^*})\left(1-\frac{q^2}{m_B^2}\right)\frac{1}{A_1(q^2)}\right)\\ &\left.\times\frac{\alpha_s C_F}{4\pi}\frac{\pi^2}{N_c}\frac{f_B f_{K^*,\perp}\lambda_{B,+}^{-1}}{m_B}\int_0^1 du\Phi_{K^*,\perp}(u)T_{\perp,+}^{(\text{nf})}(u)\right],\end{aligned} \tag{8}$$

where $\Phi_{K^*,\perp}$ is the transverse twist-2 DA for K^*. The NLO contribution in Eq. (8) is directly sensitive to this DA, and therefore it would be interesting to examine its relative significance.

Our prediction for A_{FB} distribution is given in Fig. 4 in which the latest data points from LHCb, including the zero-crossing point $q_0^2 = 3.7^{+0.8}_{-1.1}$ GeV^2 [8], and CMS [9] are shown as well.

IV. RESULTS

The AdS/QCD predictions for the $B \to K^*\mu^+\mu^-$ differential branching ratio are shown in Fig. 3. We can see that the resonance effects are significant and improve the agreement with the experimental data for q^2 regions above m_ψ^2. The gray bands in this figure (and in all

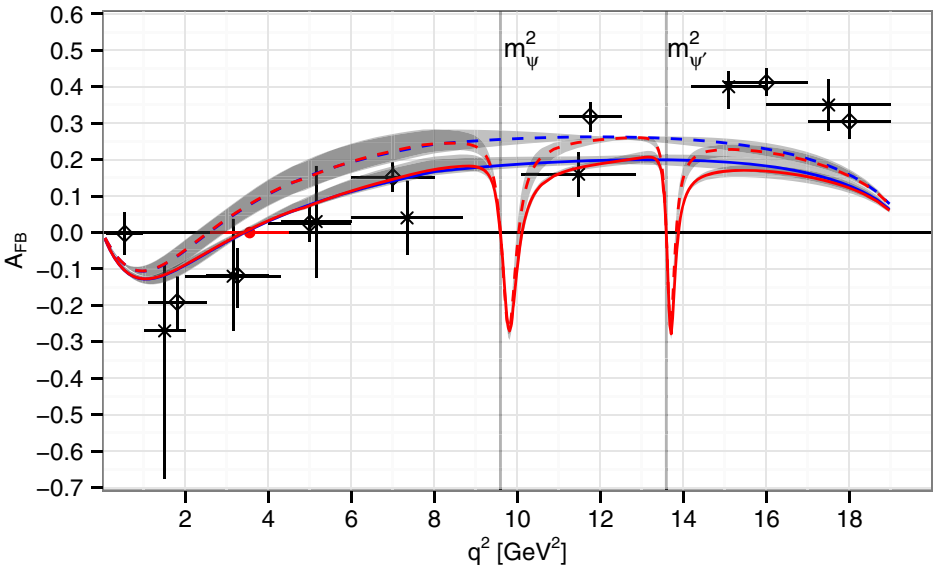

FIG. 4 (color online). Leading-order (dashed) and NLO (solid) predictions for A_{FB} including (red) and excluding (blue) the resonance effects. We compare to the latest LHCb (diamonds) and CMS (crosses) data. Note that this plot is qualitative, and our predictions for each experimental bin for this observable are shown in Table VI in Appendix.

subsequent figures) represent the uncertainty due to the renormalization scale μ (taken in the range $m_b/2 \leq \mu \leq 2m_b$) and the error bars on the lattice data for the form factors. The latter is dominated by the uncertainty in A_2 lattice calculations. Figure 5(a) shows our prediction for the differential branching ratio when we assume a momentum-independent decay constant for ψ and ψ' (dashed curve). We note from this graph that the only significant difference occurs at q^2 below the first resonance. As is the case for the inclusive $B \to X_s \ell^+ \ell^-$ [22],

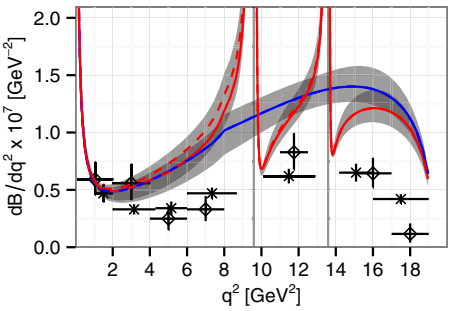

(a) The differential branching ratio using q^2-dependent (solid) and q^2-independant (dashed) f_V.

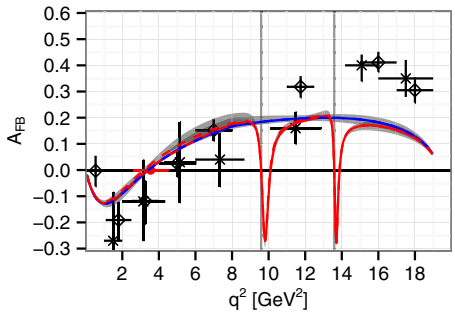

(b) A_{FB} using q^2-dependent (solid) and q^2-independant (dashed) f_V.

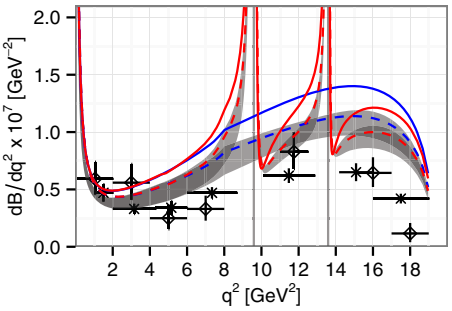

(c) The differential branching ratio within the SM (solid) and with new physics $(C_9^{\rm NP}, C_7^{\rm NP}) = (-1.0, -0.01)$ (dashed). The bin by bin predictions are given in the Appendix.

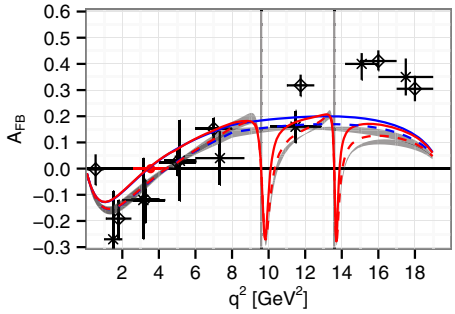

(d) A_{FB} within the SM (solid) and with new physics $(C_9^{\rm NP}, C_7^{\rm NP}) = (-1.0, -0.01)$ (dashed). The bin by bin predictions are given in the Appendix.

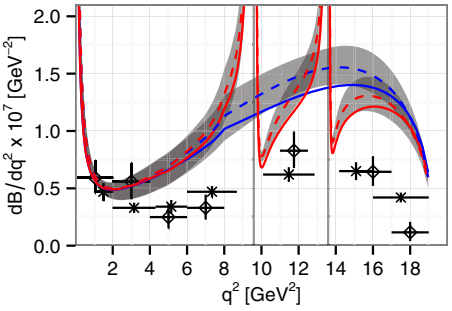

(e) The differential branching ratio using AdS/QCD (solid) and SR (dashed) DAs.

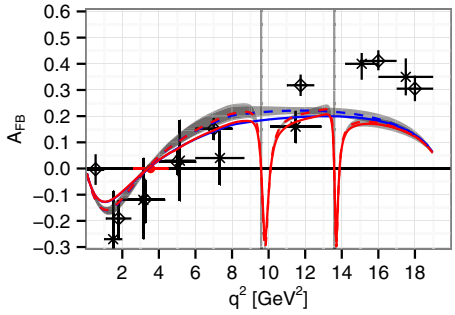

(f) A_{FB} using AdS/QCD (solid) and SR (dashed) DAs.

FIG. 5 (color online). Variations in the AdS/QCD predictions of the differential branching ratio and $A_{\rm FB}$ as explained in each figure caption. The red and blue curves show the results with and without the inclusion of ψ and ψ' resonances.

assuming momentum-dependent decay constants lead to better agreement with the experimental data for small q^2. Figure 5(c), on the other hand, shows our predictions for the differential branching ratio when additional NP contributions are added to the Wilson coefficients C_7^{eff} and C_9^{eff}. We note that assuming $C_9^{\text{NP}} = -1.0$ and $C_7^{\text{NP}} = -0.01$, as suggested by the authors of Ref. [33], produces better agreement with the data, especially at high q^2. In Fig. 5(e), we compare our predictions with those obtained from sum rules (SR) DAs. It seems that AdS/QCD DAs produce results generally lower than those obtained from SR DAs [34], especially for larger q^2. The predictions for each experimental bin for this observable are shown in Table V in the Appendix.

Our predictions for A_{FB} are shown in Fig. 4. First, we observe that the leading-order predictions miss all but one of the experimental data points as well as the zero-crossing point. Second, as pointed out in Ref. [31], the inclusion of NLO contributions leads to a significant shift to the zero-crossing point (of order 30%) and an overall better agreement with the most recent data on A_{FB} below the first resonance. We observe that the inclusion of the two resonances does not have any noticeable effects for this observable outside the resonance regions. Consequently, as shown in Fig. 5(b), assuming momentum-independent decay constants for ψ and ψ' does not change our predictions significantly. On the other hand, assuming the NP contributions $C_9^{\text{NP}} = -1.0$ and $C_7^{\text{NP}} = -0.01$ produces much better agreement with the experimental data, as seen in Fig. 5(d). Finally, predictions for A_{FB} based on AdS/QCD DAs are more or less in similar agreement with the data as those obtained from SR DAs, as illustrated in Fig. 5(f). The predictions for each experimental bin for this observable are shown in Table VI in the Appendix.

V. CONCLUSION

We used the form factors and DAs as predicted by the AdS/QCD correspondence and we have taken into account the possible $c\bar{c}$ resonance contributions to give predictions for the $B \to K^* \mu^+ \mu^-$ differential branching ratio and forward-backward asymmetry. The inclusion of ψ and ψ' resonances is done by using the Breit-Wigner model with momentum-dependent decay constants. This leads to better agreement with the experiment data for the differential decay rate outside the resonance regions. However, the forward-backward asymmetry outside the resonance region is not affected by the presence of resonances. We confirm that a negative contribution to C_9 and a small contribution to C_7, as suggested in Refs. [11,33], leads to better agreement with the experimental data. Comparison of predictions from AdS/QCD DAs and SR DAs shows that the former produces better or identical results when compared with experimental data on the branching ratio and A_{FB}. It would be interesting to investigate the use of our AdS/QCD form factors and DAs to compute other angular observables associated with $B \to K^* \mu^+ \mu^-$ decay for the whole range of q^2, in particular, the observable P_5' for which there is a discrepancy between the theory predictions and the LHCb measurement [35].

ACKNOWLEDGMENTS

This research is supported by a team grant from the Natural Sciences and Engineering Research Council of Canada. D. H. and S. L. thank the government of New Brunswick for SEED-COOP funding. The authors would also like to thank the Advanced Technology Research Group and Andy Couturier at l'Université de Moncton for their technical support. We also thank Alec Morrison for useful discussions.

APPENDIX: NUMERICAL INPUTS AND BIN BY BIN RESULTS

Throughout our analysis, we have used the input parameters presented in Table III where all quark, meson and the intermediate boson masses, as well as the experimental value of $\alpha_s(m_Z)$, are taken from the latest Review of Particle Physics [36]. The two K^* decay constants, f_{K^*} and $f_{K^*}^{\perp}$, are AdS/QCD predictions which are dependent on the masses of the quarks in the K^* meson [25].

We use the next-to-next-to-leading-order evolution for the strong coupling constant α_s which can be found in the Appendix of Ref. [37]. We also present the values of the ten Wilson coefficients at scale $\mu = m_b$ in Table IV. The complete set of equations used to obtain these values has been collected in the Appendix of Ref. [38].

TABLE V. Bin by bin values of the branching ratio defined as $\frac{10^7}{q_2^2-q_1^2}\times\int_{q_1^2}^{q_2^2}\frac{dB}{dq^2}dq^2$ for $[q_1^2, q_2^2]$ bin, with and without resonances as well as new physics contributions as compared with the latest LHCb [1] and CMS [9] data.

q^2 bin (GeV^2)	$\langle dB/dq^2\rangle$	$\langle dB^{\rm res}/dq^2\rangle$	$\langle dB^{\rm NP}/dq^2\rangle$	$\langle dB^{\rm NP,res}/dq^2\rangle$	Experiment	Process
$[0.10-2.00]$	$0.776^{-0.044}_{+0.076}$	$0.778^{-0.044}_{+0.075}$	$0.767^{-0.050}_{+0.078}$	$0.768^{-0.051}_{+0.079}$	$0.592^{+0.184}_{-0.170}$	
$[2.00-4.00]$	$0.523^{+0.044}_{-0.037}$	$0.527^{+0.045}_{-0.037}$	$0.452^{+0.047}_{-0.045}$	$0.455^{+0.046}_{-0.061}$	$0.559^{+0.197}_{-0.182}$	
$[4.00-6.00]$	$0.664^{+0.070}_{-0.063}$	$0.665^{+0.070}_{-0.063}$	$0.552^{+0.072}_{-0.068}$	$0.553^{+0.072}_{-0.080}$	$0.249^{+0.127}_{-0.113}$	
$[6.00-8.00]$	$0.869^{+0.103}_{-0.097}$	$0.930^{+0.111}_{-0.105}$	$0.709^{+0.102}_{-0.096}$	$0.755^{+0.112}_{-0.092}$	$0.330^{+0.136}_{-0.123}$	$B^+\to K^{*+}\mu^+\mu^-$ (LHCb)
$[11.00-12.50]$	$1.286^{+0.141}_{-0.133}$	$1.174^{+0.128}_{-0.121}$	$1.043^{+0.137}_{-0.130}$	$0.966^{+0.117}_{-0.081}$	$0.828^{+0.214}_{-0.197}$	
$[15.00-17.00]$	$1.370^{+0.135}_{-0.123}$	$1.198^{+0.116}_{-0.105}$	$1.114^{+0.145}_{-0.138}$	$0.990^{+0.118}_{-0.081}$	$0.644^{+0.173}_{-0.159}$	
$[17.00-19.00]$	$1.072^{+0.030}_{-0.125}$	$0.984^{+0.029}_{-0.114}$	$0.872^{+0.027}_{-0.050}$	$0.807^{+0.026}_{-0.051}$	$0.116^{+0.099}_{-0.084}$	
$[1.00-2.00]$	$0.510^{-0.005}_{+0.010}$	$0.512^{-0.005}_{+0.010}$	$0.473^{-0.009}_{+0.024}$	$0.475^{-0.008}_{+0.023}$	$0.47^{+0.076}_{-0.076}$	
$[2.00-4.30]$	$0.532^{+0.046}_{-0.040}$	$0.535^{+0.047}_{-0.040}$	$0.458^{+0.020}_{-0.030}$	$0.461^{+0.020}_{-0.030}$	$0.33^{+0.045}_{-0.045}$	
$[4.30-6.00]$	$0.676^{+0.065}_{-0.053}$	$0.677^{+0.065}_{-0.053}$	$0.561^{+0.052}_{-0.045}$	$0.562^{+0.052}_{-0.045}$	$0.34^{+0.058}_{-0.058}$	
$[6.00-8.68]$	$0.914^{+0.106}_{-0.100}$	$1.031^{+0.120}_{-0.115}$	$0.743^{+0.089}_{-0.082}$	$0.834^{+0.095}_{-0.082}$	$0.47^{+0.050}_{-0.050}$	$B^0\to K^{*0}\mu^+\mu^-$ (CMS)
$[10.09-12.86]$	$1.396^{+0.138}_{-0.121}$	$1.148^{+0.109}_{-0.094}$	$1.027^{+0.106}_{-0.091}$	$0.922^{+0.078}_{-0.063}$	$0.62^{+0.064}_{-0.064}$	
$[14.18-16.00]$	$1.164^{+0.300}_{-0.115}$	$1.058^{+0.290}_{-0.104}$	$1.135^{+0.027}_{-0.089}$	$0.960^{+0.027}_{-0.079}$	$0.65^{+0.078}_{-0.078}$	
$[16.00-19.00]$	$1.164^{+0.300}_{-0.115}$	$1.058^{+0.290}_{-0.104}$	$0.946^{+0.027}_{-0.089}$	$0.868^{+0.027}_{-0.079}$	$0.42^{+0.042}_{-0.042}$	

TABLE VI. Bin by bin values of $A_{\rm FB}$ defined as $\frac{1}{q_2^2-q_1^2}\times\int_{q_1^2}^{q_2^2}\frac{dA_{\rm FB}}{dq^2}dq^2$, with and without resonances as well as new physics contributions as compared with the latest LHCb [8] and CMS [9] data.

q^2 bin (GeV^2)	$\langle A_{\rm FB}\rangle$	$\langle A_{\rm FB}^{\rm res}\rangle$	$\langle A_{\rm FB}^{\rm NP}\rangle$	$\langle A_{\rm FB}^{\rm res,NP}\rangle$	Experiment	Process
$[0.10-0.98]$	$-0.096^{-0.003}_{+0.010}$	$-0.095^{-0.003}_{+0.010}$	$-0.103^{-0.005}_{+0.012}$	$-0.103^{-0.005}_{+0.010}$	$-0.003^{+0.058}_{-0.060}$	
$[1.10-2.50]$	$-0.099^{+0.011}_{-0.016}$	$-0.097^{+0.011}_{-0.017}$	$-0.140^{+0.010}_{-0.020}$	$-0.138^{+0.010}_{-0.021}$	$-0.191^{+0.070}_{-0.079}$	
$[2.50-4.00]$	$-0.011^{+0.010}_{-0.005}$	$-0.010^{+0.010}_{-0.005}$	$-0.065^{+0.014}_{-0.017}$	$-0.063^{+0.014}_{-0.017}$	$-0.118^{+0.075}_{-0.088}$	
$[4.00-6.00]$	$0.075^{+0.005}_{-0.020}$	$0.075^{+0.005}_{-0.020}$	$0.025^{+0.010}_{-0.009}$	$0.025^{+0.010}_{-0.007}$	$0.025^{+0.050}_{-0.050}$	$B^0\to K^{*0}\mu^+\mu^-$ (LHCb)
$[6.00-8.00]$	$0.141^{-0.007}_{+0.029}$	$0.146^{-0.012}_{+0.031}$	$0.103^{+0.009}_{-0.018}$	$0.113^{+0.006}_{-0.019}$	$0.152^{+0.041}_{-0.041}$	
$[11.00-12.50]$	$0.197^{-0.011}_{+0.012}$	$0.182^{-0.015}_{+0.020}$	$0.153^{+0.005}_{-0.005}$	$0.140^{+0.004}_{-0.005}$	$0.318^{+0.041}_{-0.041}$	
$[15.00-17.00]$	$0.181^{-0.015}_{+0.019}$	$0.166^{-0.014}_{+0.017}$	$0.104^{-0.012}_{+0.012}$	$0.123^{-0.008}_{+0.009}$	$0.411^{+0.041}_{-0.036}$	
$[17.00-19.00]$	$0.123^{-0.012}_{+0.012}$	$0.117^{-0.011}_{+0.011}$	$0.082^{-0.010}_{+0.009}$	$0.091^{-0.009}_{+0.008}$	$0.305^{+0.049}_{-0.050}$	
$[1.00-2.00]$	$-0.114^{-0.010}_{+0.016}$	$-0.113^{-0.010}_{+0.016}$	$-0.150^{-0.007}_{+0.010}$	$-0.148^{-0.009}_{+0.011}$	$-0.27^{+0.184}_{-0.406}$	
$[2.00-4.30]$	$-0.018^{+0.010}_{-0.006}$	$-0.017^{+0.010}_{-0.006}$	$-0.071^{+0.013}_{-0.017}$	$-0.069^{+0.013}_{-0.016}$	$-0.12^{+0.158}_{-0.149}$	
$[4.3-6.00]$	$0.081^{+0.005}_{-0.022}$	$0.081^{+0.005}_{-0.022}$	$0.032^{+0.010}_{-0.011}$	$0.032^{+0.010}_{-0.011}$	$0.03^{+0.153}_{-0.153}$	
$[6.00-8.68]$	$0.149^{+0.007}_{-0.029}$	$0.154^{+0.008}_{-0.030}$	$0.113^{+0.006}_{-0.022}$	$0.126^{+0.006}_{-0.027}$	$0.04^{+0.101}_{-0.101}$	$B^0\to K^{*0}\mu^+\mu^-$ (CMS)
$[10.09-12.86]$	$0.195^{-0.011}_{+0.012}$	$0.161^{-0.005}_{+0.005}$	$0.165^{+0.011}_{-0.014}$	$0.109^{+0.006}_{-0.019}$	$0.16^{+0.061}_{-0.061}$	
$[14.18-16.00]$	$0.192^{-0.015}_{+0.019}$	$0.163^{-0.011}_{+0.014}$	$0.163^{+0.008}_{-0.010}$	$0.109^{+0.008}_{-0.007}$	$0.40^{+0.041}_{-0.061}$	
$[16.00-19.00]$	$0.140^{-0.013}_{+0.014}$	$0.131^{-0.012}_{+0.013}$	$0.118^{-0.010}_{+0.010}$	$0.102^{-0.021}_{+0.007}$	$0.35^{+0.071}_{-0.071}$	

[1] R. Aaij *et al.* (LHCb Collaboration), J. High Energy Phys. 06 (2014) 133.
[2] T. Aaltonen *et al.* (CDF Collaboration), Phys. Rev. Lett. **108**, 081807 (2012).
[3] J. Lees *et al.* (*BABAR* Collaboration), Phys. Rev. D **86**, 032012 (2012).
[4] J.-T. Wei *et al.* (BELLE Collaboration), Phys. Rev. Lett. **103**, 171801 (2009).
[5] R. Aaij *et al.* (LHCb Collaboration), Phys. Rev. Lett. **111**, 191801 (2013).
[6] R. Aaij *et al.* (LHCb Collaboration), J. High Energy Phys. 07 (2012) 133.
[7] R. Aaij *et al.* (LHCb Collaboration), J. High Energy Phys. 08 (2013) 131.
[8] C. Langenbruch, K. Petridis, and N. Serra (LHCb Collaboration), Report No. LHCb-CONF-2015-002 (2015).
[9] V. Khachatryan *et al.* (CMS Collaboration), arXiv:1507.08126.
[10] W. Altmannshofer and D. M. Straub, Eur. Phys. J. C **73**, 2646 (2013).
[11] S. Descotes-Genon, J. Matias, and J. Virto, Phys. Rev. D **88**, 074002 (2013).
[12] T. Hurth and F. Mahmoudi, J. High Energy Phys. 04 (2014) 097.
[13] S. Descotes-Genon, T. Hurth, J. Matias, and J. Virto, J. High Energy Phys. 05 (2013) 137.
[14] R. Gauld, F. Goertz, and U. Haisch, Phys. Rev. D **89**, 015005 (2014).
[15] A. J. Buras and J. Girrbach, J. High Energy Phys. 12 (2013) 009.
[16] R. Gauld, F. Goertz, and U. Haisch, J. High Energy Phys. 01 (2014) 069.
[17] C. Hambrock, G. Hiller, S. Schacht, and R. Zwicky, Phys. Rev. D **89**, 074014 (2014).
[18] A. Khodjamirian, T. Mannel, A. Pivovarov, and Y.-M. Wang, J. High Energy Phys. 09 (2010) 089.
[19] A. Bharucha, T. Feldmann, and M. Wick, J. High Energy Phys. 09 (2010) 090.
[20] A. Datta, M. Duraisamy, and D. Ghosh, Phys. Rev. D **89**, 071501 (2014).
[21] A. K. Alok, A. Dighe, D. Ghosh, D. London, J. Matias, M. Nagashima, and A. Szynkman, J. High Energy Phys. 02 (2010) 053.
[22] M. R. Ahmady, Phys. Rev. D **53**, 2843 (1996).
[23] K. Terasaki, Nuovo Cimento A **66**, 475 (1981).
[24] J. Lyon and R. Zwicky, Phys. Rev. D **88**, 094004 (2013).
[25] M. Ahmady, R. Campbell, S. Lord, and R. Sandapen, Phys. Rev. D **89**, 074021 (2014).
[26] M. Ahmady and R. Sandapen, Phys. Rev. D **88**, 014042 (2013).
[27] G. F. de Teramond and S. J. Brodsky, Phys. Rev. Lett. **102**, 081601 (2009).
[28] S. J. Brodsky, G. F. de Teramond, H. G. Dosch, and J. Erlich, Phys. Rep. **584**, 1 (2015).
[29] N. G. Deshpande, J. Trampetić, and K. Panose, Phys. Rev. D **39**, 1461 (1989).
[30] C. Lim, T. Morozumi, and A. Sanda, Phys. Lett. B **218**, 343 (1989).
[31] M. Beneke, T. Feldmann, and D. Seidel, Nucl. Phys. **B612**, 25 (2001).
[32] R. R. Horgan, Z. Liu, S. Meinel, and M. Wingate, Phys. Rev. D **89**, 094501 (2014).
[33] S. Descotes-Genon, L. Hofer, J. Matias, and J. Virto, J. Phys. Conf. Ser. **631**, 012027 (2015).
[34] P. Ball, V. M. Braun, and A. Lenz, J. High Energy Phys. 08 (2007) 090.
[35] S. Descotes-Genon, J. Matias, M. Ramon, and J. Virto, J. High Energy Phys. 01 (2013) 048.
[36] K. Olive *et al.* (Particle Data Group), Chin. Phys. C **38**, 090001 (2014).
[37] M. Ahmady and F. Mahmoudi, Phys. Rev. D **75**, 015007 (2007).
[38] M. Ahmady, S. Lord, and R. Sandapen, Phys. Rev. D **90**, 074010 (2014).